HOSTED BY

ELSEVIER

CrossMark

Available online at www.sciencedirect.com

ScienceDirect

Progress in Natural Science: Materials International 25 (2015) 291–299

Progress in Natural Science Materials International

www.elsevier.com/locate/pnsmi
www.sciencedirect.com

Original Research

Synthesis of few layer single crystal graphene grains on platinum by chemical vapour deposition

S. Karamat[a,b], S. Sonuşen[c], Ü. Çelik[d], Y. Uysallı[a], E. Özgönül[a], A. Oral[a,*]

[a]Department of Physics, Middle East Technical University, Ankara 06800, Turkey
[b]COMSATS Institute of Information Technology, Islamabad 45550, Pakistan
[c]Faculty of Engineering and Natural Sciences, Sabancı University, Istanbul 34956, Turkey
[d]NanoMagnetics Instruments Ltd., Ankara, Turkey

Received 23 February 2015; accepted 2 June 2015
Available online 31 August 2015

Abstract

The present competition of graphene electronics demands an efficient route which produces high quality and large area graphene. Chemical vapour deposition technique, where hydrocarbons dissociate in to active carbon species and form graphene layer on the desired metal catalyst via nucleation is considered as the most suitable method. In this study, single layer graphene with the presence of few layer single crystal graphene grains were grown on Pt foil via chemical vapour deposition. The higher growth temperature changes the surface morphology of the Pt foil so a delicate process of hydrogen bubbling was used to peel off graphene from Pt foil samples with the mechanical support of photoresist and further transferred to SiO_2/Si substrates for analysis. Optical microscopy of the graphene transferred samples showed the regions of single layer along with different oriented graphene domains. Two type of interlayer stacking sequences, Bernal and twisted, were observed in the graphene grains. The presence of different stacking sequences in the graphene layers influence the electronic and optical properties; in Bernal stacking the band gap can be tunable and in twisted stacking the overall sheet resistance can be reduced. Grain boundaries of Pt provides low energy sites to the carbon species, therefore the nucleation of grains are more at the boundaries. The stacking order and the number of layers in grains were seen more clearly with scanning electron microscopy. Raman spectroscopy showed high quality graphene samples due to very small D peak. 2D Raman peak for single layer graphene showed full width half maximum (FWHM) value of 30 cm^{-1}. At points A, B and C, Bernal stacked grain showed FWHM values of 51.22, 58.45 and 64.72 cm^{-1}, while twisted stacked grain showed the FWHM values of 27.26, 28.83 and 20.99 cm^{-1}, respectively. FWHM values of 2D peak of Bernal stacked grain showed an increase of 20–30 cm^{-1} as compare to single layer graphene which showed its dispersive nature and confirmed Bernal sequence. On the other hand, the slightest decrease in FWHM values of 2D peak in twisted grain comparing to single layer confirmed the twisted sequence of grains. Atomic force microscopy analysis showed an increasing trend in grain height profile with an increase in the number of layers.

Keywords: Chemical vapour deposition; Graphene hexagonal crystals; Bernal stacking; Twisted stacking; Grain boundaries and hydrogen bubbling

1. Introduction

Graphene, discovered in 2004 [1], is a monolayer of sp^2-bonded carbon atoms ordered into a two dimensional honeycomb lattice which has unique physical properties. Graphene has already generated a plethora of applications and novel phenomena in physics because of its marvellous properties: such as flexibility, high transparency, impermeability and electrical conductivity; which has potential in different applications including conductive ink [2], terahertz transistors [3], ultrafast photo detectors [4], flexible touch screens [5], strain sensors [6] and many others. Various growth methods have been developed to produce single and few layer graphene such as mechanical exfoliation [1,7], reduction of graphene oxide [8] and chemical vapour deposition (CVD) on various metal surfaces [9–11]. CVD is the most appropriate growth method

*Corresponding author. Tel.: +90 312 210 3266; fax: +90 312 210 5099.
E-mail address: orahmet@metu.edu.tr (A. Oral).
Peer review under responsibility of Chinese Materials Research Society.

http://dx.doi.org/10.1016/j.pnsc.2015.07.006

for producing large area and high quality single or multi layer graphene using catalytic substrates and hydrocarbons. Zero bandgap structure of single layer graphene limits the graphene's potential in electronic and optical applications [12] as it is not possible to make switching devices with a high on–off ratio. Therefore attention has been diverted from single layer to bilayer and trilayer graphene, in which a bandgap is formed because of the interlayer interactions. Few layer graphene with high quality and uniformity can be grown using CVD by controlling growth parameters on metallic substrates like Cu [9], Ni [10,11], Pt [13], Ir [14], Ru [15] and Au [16]. It has also been shown that multilayer graphene, grown with CVD method, can have a multiplicative effect and acts as a better diffusion barrier than single layer graphene [17]. Recently, few layer small hexagonal grains have been prepared on Cu by CVD which show different interlayer stacking orders [18]. The twisted and the Bernal [18] stacking of the graphene layers influence its electronic and optical properties. The Bernal stacking of bilayer graphene, where half of the atoms in adjacent layers lie on top of each other, can exhibit tuneability of the bandgap up to 250 meV by an external electric field; and makes graphene more useful in nanoelectronics [19–23]. The twisted stacking, where the two adjacent layers are misoriented by a certain angle do not exhibit a tuneable bandgap, but can reduce the graphene film's overall sheet resistance. It was reported that the sheet resistance of single layer graphene is about 980 $\Omega/\square$ [24], and Li et al. achieved sheet resistance of 350 $\Omega/\square$ in a stack of four layer undoped graphene with 90% optical transmittance, but the formation of cracks during their transfer onto the substrate affected the optical transmittance [25]. The twisted stacking of graphene shows promise for transparent conductive electrode applications such as OLED displays, touch screen panels and solar cells [26]; thus making CVD a plausible choice for achieving few layer graphene with same or twisted interlayer orientations.

In this study, few layer hexagonal single crystal graphene on Pt foils were synthesised using ambient CVD method. Pt foils were used as substrates for growth because of its weak interaction with the graphene, which would help in minimising the effect of the substrate on the physical properties of the graphene. An electrolysis method was used to peel off graphene layers from the Pt substrate, which was demonstrated by Gao et al. [13]. The process of creating different stacking layers in graphene is a new approach toward stacking-dependent electronics and optics; therefore it is important to understand how these interstacking orientations are formed and how they could be controlled. The graphene layers were characterised by scanning electron microscopy (SEM), Raman spectroscopy, atomic force microscopy (AFM) and optical microscopy. Bernal (AB) and twisted (anomalous) interlayer stacking in single crystal hexagons of few layer graphene were observed.

2. Experimental details

2.1. Growth of graphene

Single crystal graphene grains of different interlayer stacking were grown on Pt foils in an ambient pressure CVD (AP-CVD) system using CH_4 (99.995% purity, Messer), H_2 (99.999% purity, BOS) and Argon (99.999% purity, Messer) gases. A standard 40 mm diameter quartz tube was used as the reaction chamber in a split CVD furnace. Before loading inside the reaction chamber, the 50 μm thick 99.995% pure Pt foil was cut into dimensions of 20×15 mm pieces and was cleaned with acetone, isopropanol and deionised (DI) water. Next, it was dipped in diluted (1:10) nitric acid for three minutes followed by rinsing and blow drying. After loading the Pt foil in the reaction chamber, the CVD system was evacuated down to $\sim 5 \times 10^{-2}$ mbar pressure. The Ar gas was maintained at a flow rate of 300 sccm for 15 min and the hydrogen gas was introduced afterwards at the rate of 50 sccm. The furnace was turned on and the Ar flow was stopped at 200 °C. The hydrogen flow was increased from 50 to 150 sccm at 800 °C and was maintained at this level until the end of the experiment. When the furnace temperature reached 1040 °C, CH_4 was introduced into the system at a flow rate of 1.4 sccm for three hours to grow the graphene. After three hours of growth, furnace was opened to quickly cool down the samples. CH_4 flow was turned off after 650 °C while the hydrogen was stopped at 200 °C. The samples were cooled down in an Ar atmosphere to room temperature, which was introduced into the chamber at 200 °C.

2.2. Transfer of graphene

After the CVD growth, graphene/Pt substrate was coated with C9-PMMA electron beam resist to provide mechanical support to the graphene during transfer. PMMA layer was spin coated for 60 s at 3500 rpm, followed by curing at 180 °C for 30 min. 1 M sodium hydroxide (NaOH) solution was prepared by adding NaOH in DI water in order to exfoliate graphene layers from the Pt foil by hydrogen bubbling. PMMA/graphene/Pt substrate was attached to the negative terminal of a DC power supply and acted as a cathode; another piece of Pt foil was used as the anode. The value of electrolysis current was maintained in the range of 0.1–0.2 A at ~ 3 V. The hydrogen bubbles produced at the cathode peels the graphene/PMMA stack from the Pt surface and the graphene/PMMA stack floats on the solution [13]. The graphene/PMMA stack was scooped out of the solution using a clean glass slide and transferred to DI water for cleaning. The stack was kept in DI water for 2 min, scooped again and transferred to DI water a second time, the SiO_2 covered Si substrate was dipped into the water and finally the graphene/PMMA stack was scooped out. The sample was left overnight in air to dry. After drying, samples were heated at 180 °C on a hot plate followed by vacuum drying at 70 °C for three hours [27]. The samples were cleaned in acetone at 75 °C for 5 min to dissolve the PMMA layer, followed by a nitrogen blow dry. Fig. 1 summarises the main experimental steps mentioned in Sections 2.1 and 2.2.

2.3. Characterisation of graphene

Optical microscopes (Carl Zeiss Axio Scope A1 MaT and Nikon Eclipse LV 100) were used to inspect the graphene samples first. The samples were also imaged using Zeiss Supra 35VP field emission scanning electron microscope (FESEM).

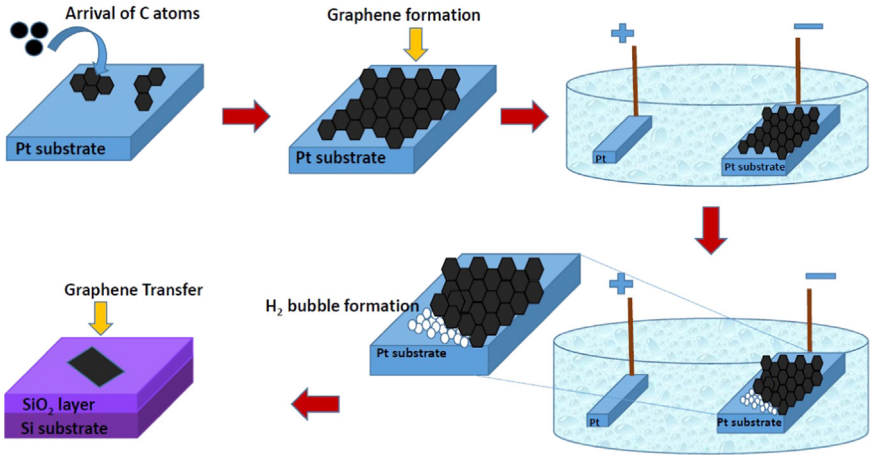

Fig. 1. Schematic illustration of graphene growth on Pt and its transfer to SiO_2/Si substrates.

Renishaw inVia Reflex microRaman spectrometer with 532 nm laser source is used to measure the Raman spectra. High Performance Atomic Force Microscope (hp-AFM) from NanoMagnetics Instruments [28] was employed for AFM analysis and to measure the thickness of graphene layers independently using PPP-NCLR cantilevers (Nanosensors) in tapping mode.

3. Results and discussion

Most of the graphene grew as a single layer on Pt with many few layer graphene single crystals in the shape of regular hexagons which were initially identified under the optical microscope. Two types of multilayer graphene grains were observed in the graphene samples; the one with similar interlayer orientation known as Bernal stacking shown in Fig. 2(a), and the other with $\sim 30^{\circ}$ interlayer orientation known as twisted (anomalous/turbo) stacking [29] is shown in Fig. 2(b).

The presence of naturally found zigzagged edges on a metallic substrate help graphene grains to grow in the form of hexagonal crystals [30], as shown in Fig. 2(c). Vapour source and type of substrate material are the two factors which play an important role in the nucleation and graphene growth. The suitable sites for nucleation are non-equilibrium defects (vacancies, grain boundaries, dislocations, and stacking faults), surface impurities and orientation of the underlying substrate. When carbon atoms arrive on the substrate surface they diffuse around and may find a nucleation site, or they may re-evaporate. The probability of sticking of atoms depends on many factors such as: energy of the carbon species, angle of their arrival at the substrate, type of substrate etc. When carbon atoms reach to the surface, they stay either on the point where they first arrived or they move around on the surface with diffusion. When the atoms arrive on the surface they move on the surface until they reach a position that minimises the total energy. The atoms move around until they find the lowest energy nucleation site. The defects on the substrate always have steps and they act as an effective nucleation sites compared to other locations. The size of the nucleated domains increases with the arrival of new atoms at the surface [31].

The graphene growth is due to carbon solubility in copper and platinum and both metals are considered as good catalysts for graphene growth [18]. For Cu, it was reported that graphene growth is a self mediated process, where hydrocarbons partially dehydrogenate into carbon species ($CH_{x=0-3}$), they diffuse into the active sites on the substrate, nucleate and then grow from islands to domains [32,33]. These domains grow in size by adsorbing more carbon species on their edges. The abovementioned process was followed by carbon species to diffuse and nucleate on Pt surface as well [33].

The growth of regular pattern stacked layers is dependent on growth parameters and morphology of the growing substrate. The fast nucleation density of carbon species on metal substrates produces small grains of few layer graphene [34,35]. In order to get clear information about the surface morphology of the graphene sample, FESEM was used. Fig. 3(a) and (b) and Fig. 4(a) and (b), show few layers of graphene hexagons of different sizes stacked at each other.

It is imperative to understand how these hexagons arrange themselves systematically. Few reports show that the smaller layers of graphene on Cu arrange on the top of the larger layers, like a tiered wedding cake [36,37]. Crystal growth mechanism for other materials also support this stacking sequence of layers where the layers always nucleate and grow on the topside of the crystal. It means, the smaller layer will nucleate on top of the first layer, the next smaller layer will grow on the top of the previous layer and pyramidal stacking of layers will form [38]. However, in the case of graphene it is different, Tontegoe et al. reported inverted wedding cake structure for the graphene growth on the basis of their Auger electron spectroscopy results, and it was observed that the second and subsequent layers of graphene were grown next to the substrate [39]. Recent studies also confirm the growth mechanism of graphene layers happen underneath the first layer instead of top of the first monolayer [40–42]. The active carbon species contribute to the growth of bilayer graphene by diffusing across the edges of the first single layer graphene. In a growth process, most of the carbon species take part in the growth of the first layer and only a small amount of them would be able

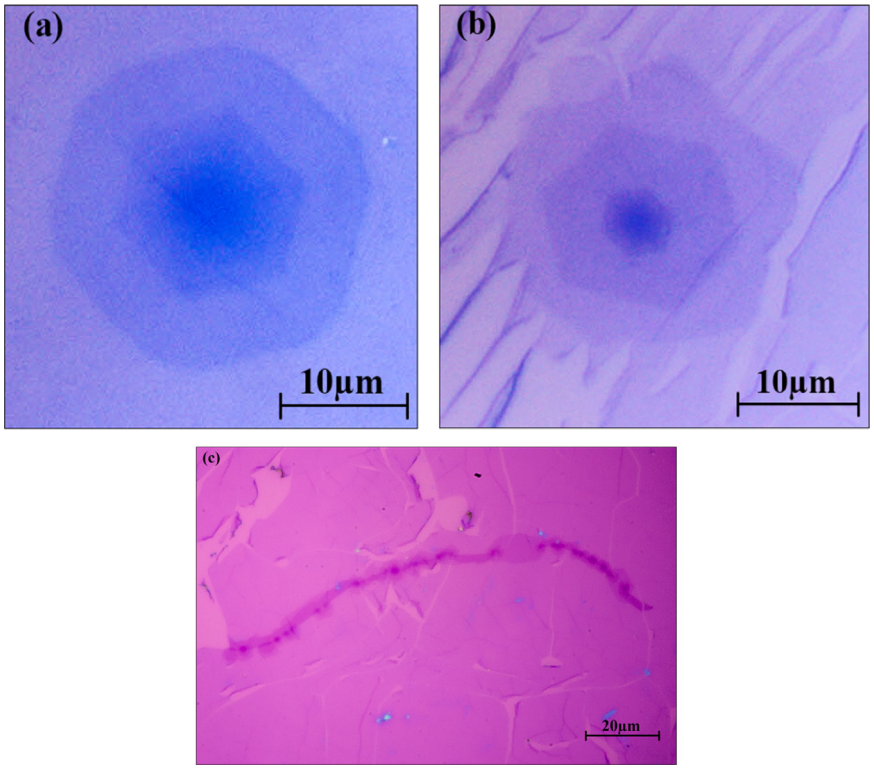

Fig. 2. (a) Optical microscope image for single crystal graphene hexagon of Bernal interlayer stacking, (b) anomalous interlayer stacking and (c) nucleation sites at grain edges.

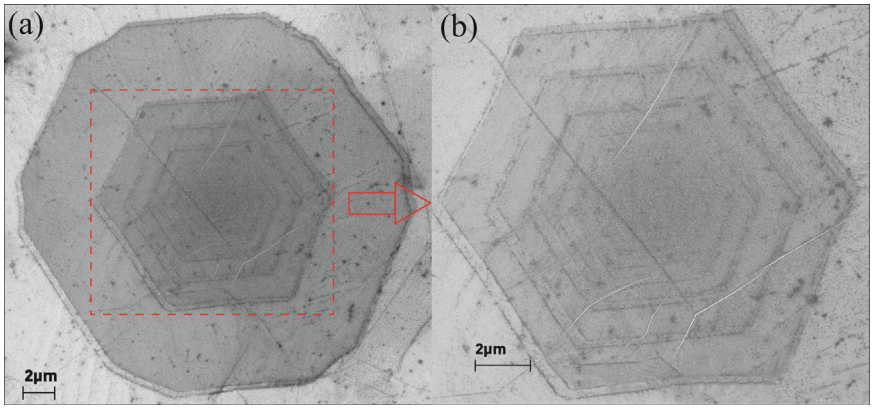

Fig. 3. (a) SEM image of the grain having Bernal stacking. (b) Magnified SEM image of the central part of grain to get information about number of layers.

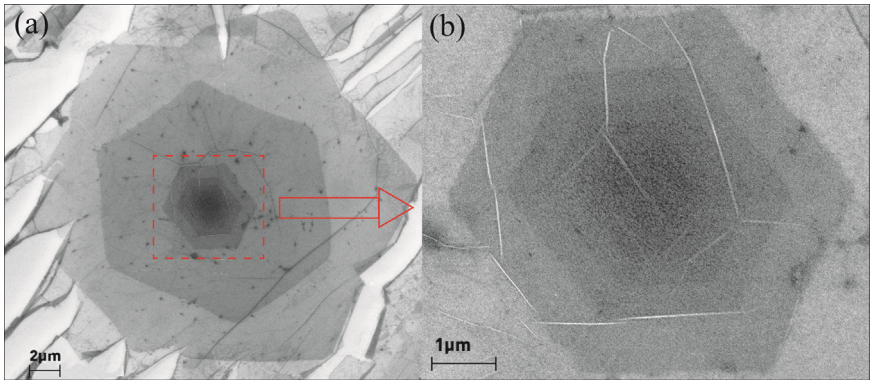

Fig. 4. (a) SEM image of the grain having twisted stacking (b) Magnified SEM image of the central part of grain to get information about number of layers.

to enter from the edges of this layer and nucleate on the metal surface thus contributing in bilayer growth. The super saturation of carbon species increases their chances to cross the edges of the first layer and contribute to the growth of the second layer [37]. The images of grains shown in Figs. 3 and 4 reveal that the central active site is same for all the layers of hexagons and they nucleate from it at different times. In the under layer mechanism, new layers nucleate next to the substrate, so the site remains active even when covered by graphene.

The band structure of graphene is sensitive to the number of layers and their stacking sequence. The interlayer interactions for the same number of graphene layers vary if they are arranged in Bernal or twisted configurations which change their optical and transport properties. It is important to understand the graphene layers structure and their stacking sequence. Raman spectroscopy is the best tool for taking non-destructive measurements. The general features of graphene in the Raman spectrum appear in the range of 1000–3000 cm^{-1} with characteristic peaks D, G and 2D at around ~1350, ~1560 and ~2700 cm^{-1}, respectively. The G peak represents the E_{2g} phonon of the Brillouin zone centre, while the D peak corresponds to the breathing modes of sp^2 atoms and it is activated when the defects are present in graphene. D peak comes from the transverse optical (*TO*) phonons existing around the *K* point of the Brillouin zone. D peak becomes active by double resonance phenomena and its intensity profile is attributed to the amount of disorder, but it won't give information about the number of graphene layers. The 2D or G ´ peak arises from the scattering of two phonons with the equal but opposite wave vector phonons. In the first Brillouin zone, Raman double resonance phenomena involves two phonons and electronic states which lies near two non-equivalent K points and create 2D peak in the Raman spectrum [43–45]. The D peak is weak for highly crystalline samples, on the other hand, 2D peak which is an overtone of D peak always exist even when its first order is absent. A very weak D peak was observed in the spectra which showed high crystalline nature of few layer graphene grains.

Figs. 5 and 6 show Raman spectra of single layer and differently stacked graphene grains at different points obtained using 532 nm as the excitation wavelength (2.33 eV laser energy). Raman spectrum for single layer graphene was measured at different points on the sample, one of them is shown in Fig. 3 of the supporting information. The changes in shape and peak position of the 2D peak with the change in the number of graphene layers were clearly observed. Fig. 5 shows the Raman spectra for Bernal stacked hexagonal layers of graphene. Generally, 2D peak is a secondary D peak and having largest intensity in single layer graphene, it broadens into four peaks due to double resonance scattering and reduces in intensity in multi layer graphene. The reason is well reported previously, the single layer graphene exhibits a symmetrical peak and can be fitted with one Lorentzian peak because of the single electron valence (π) and conduction (π^*) band structure. For this structure, one scattering cycle is excited near the K and K´ points and the full width at half maximum (FWHM) of single layer is ~ 26.3 cm^{-1} [46]. In the case of bilayer, the interaction of planes divide π and π^* electronic bands into four parabolic band structures (π_1, π_2, π_1^*, π_2^*). The space group theory explains that the laser light excite electrons in the form of pairs (π_1, π_1^* and π_2, π_2^*) among the four band structures. It makes the 2D peak dispersive for bilayer graphene and it can be fitted with four Lorentzian peaks for bilayer Bernal stacked graphene the FWHM reaches almost twice that of the single layer graphene. For tri and tetra layer graphene, the splitting of the electronic bands becomes more complex and dispersive which cause further widening of the 2D peaks [46,47].

The asymmetry in the 2D peak for different layers can be seen, as shown in Fig. 5(b). The number of layers changes the shape of 2D peak which hint towards the change in electronic band structure and the phonon dispersion. It is well reported that when the graphene layers exceed more than five in number, the 2D peak looks like a graphite peak [44]. 2D peak for multilayer hexagonal structures at points A, B and C are assumed to be for bi-, tri- and multi-layer graphene, and were fitted with four peaks along with single layer graphene, as shown in Fig. 5(c–f). The values of FWHM for fitted 2D peak at points A, B and C are 51.22, 58.45 and 64.72 cm^{-1}, respectively. FWHM values show an increase with the increase in number of layers, as shown in Fig. 5(g) and are also twice that of the single layer graphene FWHM value (~30 cm^{-1}). The values of peak position for points A, B and C are 2703.73, 2705.07 and 2713.16 cm^{-1}, respectively. The peak positions also show a blue shift with an increase in the number of graphene layers. The value of 2D peak for Bernal stacking is greater than 50 cm^{-1} which clearly shows AB stacking sequence in graphene layers [48]. Moreover, the normalised I_{2D}/I_G ratio for points A, B and C is 0.47, 0.40 and 0.37, respectively. The smaller intensity ratios hint towards the Bernal stacked layers [48]. The Raman spectra provides information about the number of layers and interlayer stacking sequence in hexagonal crystals of graphene.

Fig. 6 shows the Raman spectra for twisted layers of hexagonal graphene crystal. The 2D Raman peak which is sensitive to band structure shows complicated behaviour for twisted layer graphene. It is well reported that when graphene samples are probed with 532 nm light, the resonance phenomena occurs at a critical angle of 12.5°. If the rotations of the stacked layers are greater than this value then the G mode intensity varies as a Lorentzian function and 2D peak for few layer graphene resembles the Raman spectrum of single layer graphene [49,50]. The twisted grain had an orientation of ~ 30° shown in supporting information Fig. 1. The 2D peak was fitted for points A, B and C with four peaks shown in Fig. 6 (c)–(e). For points A, B and C, the FWHM value of 2D peaks is 27.26, 28.83 and 20.99 cm^{-1}, respectively. These values are very close to the findings of Li et al. [48] where the values of 2D peak for twisted bilayers graphene was ~ 31 cm^{-1} and for monolayer graphene around 37 cm^{-1}.

In the present investigation, the FWHM value of single layer graphene is 30 cm^{-1},and with the increase in number of

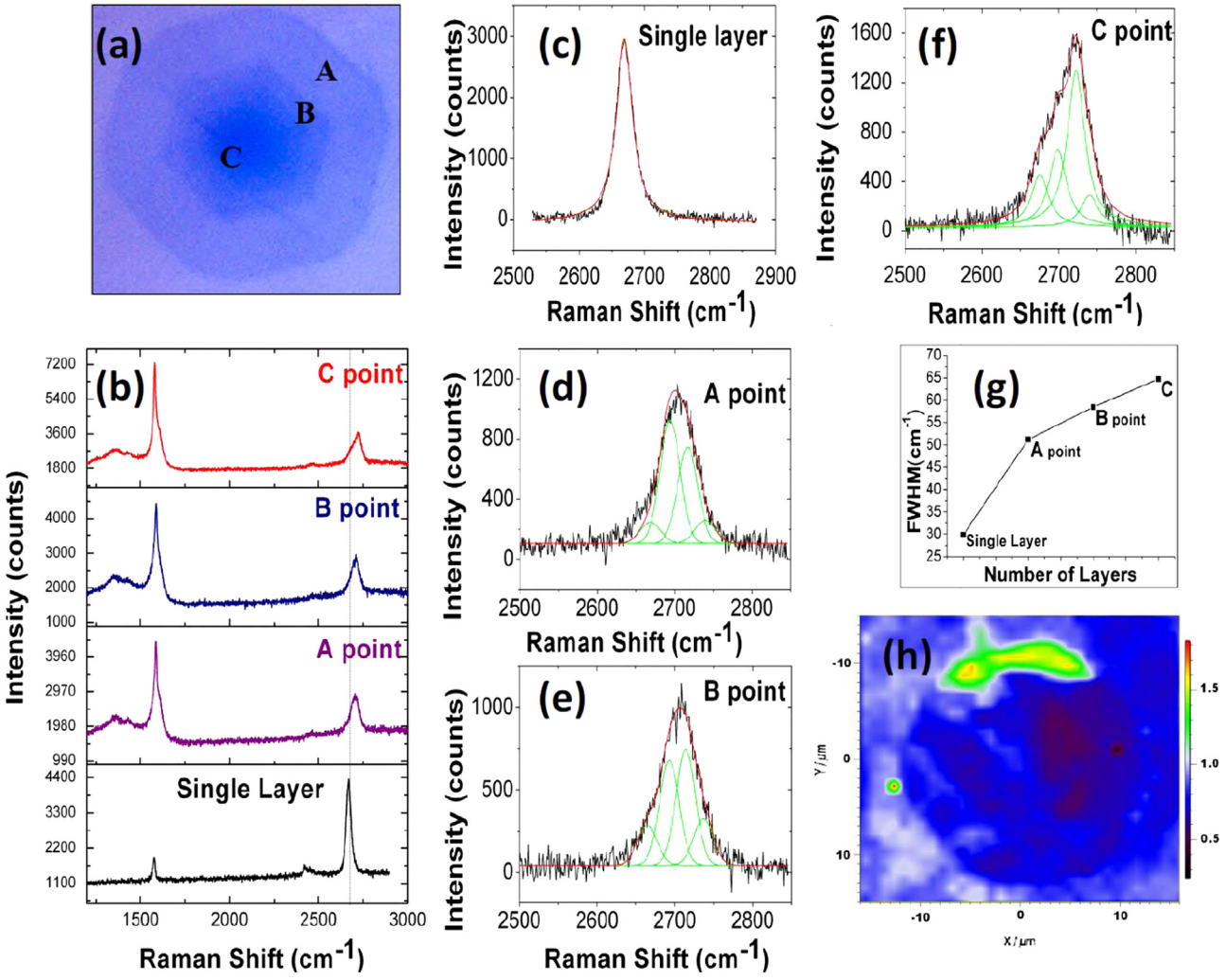

Fig. 5. (a) Marked optical image of graphene hexagon for Raman spectrum at different points, (b) Raman spectra for Bernal (AB) stack hexagons of graphene at points A, B and C and single layer graphene, (c) Fitted spectra of 2D peak for single layer graphene, (d) 2D peak fitted with four peaks at point A, (f) 2D peak fitted with four peaks at point B, (f) 2D peak fitted with four peaks at point C, (g) Increasing trend of FWHM of 2D peaks with the increase in number of layers (single layer, point A, B and C) and (h) Raman mapping of Bernal stacked grain.

twisted layers, FWHM values show a decrease with respect to single layer graphene. It is worthy to note here that the FWHM values of twisted layer graphene is significantly lower than that of Bernal stacked layers, indicating that the electronic band structures is not widening. In twisted layers, the π electrons follow different evolution rules from the Bernal stacked few layer graphene. Theoretically, the twisted graphene layers exhibit electronic structure similar to single layer graphene but with lesser Fermi velocity, which means smaller slope of electronic band near *K* points [49]. Moreover, the values of peak position for single layer graphene and points A, B and C are 2669.12, 2693.86, 2697.76 and 2698.50 cm^{-1}, respectively. The peak positions also show a blue-shift with an increase in the number of graphene layers. The normalised I_{2D}/I_G ratio for points A, B and C is 1.92, 2.76 and 7.89, respectively, which is quite higher than the values of Bernal stacked graphene layers. The higher intensity ratios hint towards the twisted stacked layers [48,50].

AFM images of the few layer graphene grains are shown in Fig. 7(a) and (b). hp-AFM from NanoMagnetics Instruments and PPP-NCLR AFM cantilevers having a nominal resonant frequency of ∼ 190 kHz were used in tapping mode. The height of graphene grains lies between 2–5 nm (Figs. S4 and S5 of Supporting information). The height profile images show an increasing trend with the increase in number of layers. It is worthy to mention here that the interlayer spacing of graphite is 3.35 Å but the first layer is always measured as ∼ 1 nm, similar to the literature [29]. The single layer graphene on 285 nm SiO_2/Si substrate show a step height of 1.2–1.58 nm at different points. This value is in good agreement with the known interlayer spacing for graphite layers and also suggest AB stacking [51,52]. The effect mentioned above increases the thickness of a graphene layer on the substrate and it's not a very precise way to get information about the exact height of graphene grains but it can give a clear indication of an increasing trend in height with the increase in number of layers shown in Figs. S4 and S5 of Supporting information.

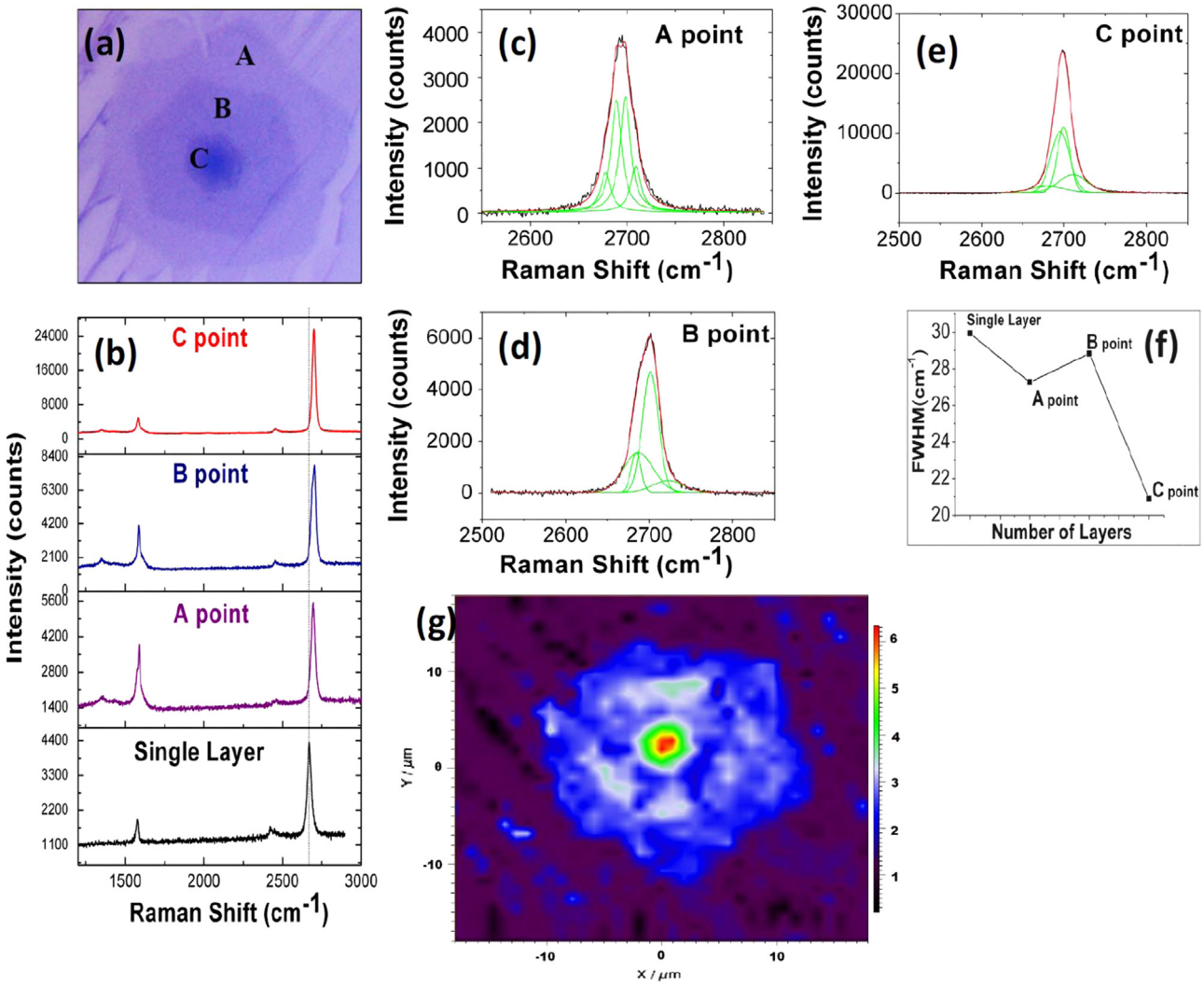

Fig. 6. (a) Marked optical image of graphene hexagon for Raman spectrum at different points (b) Raman spectra for twisted stacking hexagons of graphene at points A, B and C, (c) 2D peak fitted with four peaks at point A, (d) 2D peak fitted with four peaks at point B, (e) 2D peak fitted with four peaks at point C, and (f) Increasing trend of FWHM of 2D peaks with the increase in number of layers (single layer, point A, B and C) and (g) Raman mapping of the twisted hexagon.

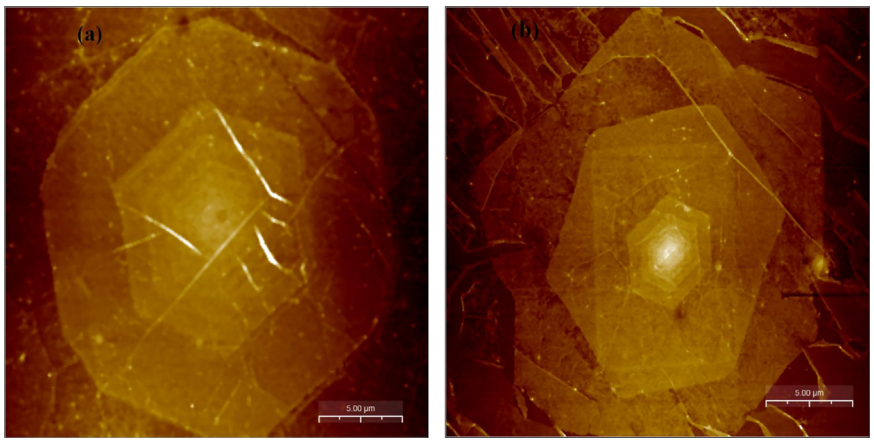

Fig. 7. (a) AFM image for Bernal stacked grain, (b) for twisted grain.

4. Conclusion

In the present work, the single layer graphene with few layer single crystal grains were synthesised on Pt foils using CVD. Different characterizations were done to analyse the single layer graphene and the interlayer orientation of different grains. The most frequent interlayers orientations observed in few layer single crystals of ~ 25 μm in size were AB Bernal and twisted stacking. Optical images gave the preliminary information about the graphene transfer on SiO_2/Si substrates after transfer. SEM analysis clearly shows crystal boundaries in the form of perfect hexagons. The presence of nucleation sites at the grain boundaries of substrate is higher due to their low energy area. Raman spectroscopy also supports the AB and twisted stacking in graphene grains. The FWHM of 2D peaks double for the AB stacking while the twisted stacking shows the FWHM near the single layer which appears at 30 cm^{-1}. Moreover, the normalised I_{2D}/I_G ratio in Bernal stacked grain for points A, B and C is 0.47, 0.40 and 0.37, respectively which support the AB interlayer orientation. In twisted stacking grain, the normalised I_{2D}/I_G ratio for points A, B and C is 1.92, 2.76 and 7.89, respectively, which is higher than the intensity ration of Bernal stacked graphene layers. This increase in intensity ratios hint towards the twisted stacked layers. AFM images show an increasing trend with the number of layers but determining the exact height of the graphene layer from the SiO_2/Si substrate is not possible. For future study, it is proposed that the size of grains can be controlled by changing the growth parameters and can create the desired stacking sequence of graphene layers which will open new ways in multilayer applications.

Acknowledgements

S. Karamat would like to thank TÜBİTAK and Marie Curie Actions Co.-Funded 2236 fellowship for accomplishing this work.

Appendix A. Supporting information

Supplementary data associated with this article can be found in the online version at http://dx.doi.org/10.1016/j.pnsc.2015.07.006.

References

[1] K.S. Novoselov, A.K. Geim, S.V. Morozov, D. Jiang, Y. Zhang, S.V. Dubonos, I.V. Grigorieva, A.A. Firsov, Science 306 (2004) 666–669.
[2] N.A. Luechinger, E.K. Athanassiou, W.J. Stark, Nanotechnology 19 (2008) 445201–445206.
[3] K.S. Novoselov, V.I. Falko, L. Colombo, P.R. Gellert, M.G. Schwab, K. Kim, Nature 490 (2012) 192–200.
[4] F. Xia, T. Mueller, Y. -ming Lin, A.V. Garcia, P. Avouris, Nat. Nanotechnol. 4 (12) (2009) 839–843.
[5] S. Bae, H. Kim, Y. Lee, X. Xu, J.-S. Park, Y. Zheng, J. Balakrishnan, T. Lei1, H.R. Kim, Y.I.l. Song, Young.-J. Kim, K.S. Kim, B. Özyilmaz, J.-H. Ahn, B.H. Hong, S. Iijima, Nat. Nanotechnol. 5 (2010) 574-8.
[6] S. Bae, Y. Lee, B.K. Sharma, H.-J. Lee, J.-H. Kim, J.-H. Ahn, Carbon 51 (2013) 236–242.
[7] A.K. Geim, K.S. Novoselov, Nat. Mater. 6 (2007) 183–191.
[8] G. Eda, G. Fanchini, M. Chhowalla, Nat. Nanotechnol. 3 (2008) 270–274.
[9] X. Li, W. Cai, J. An, S. Kim, J. Nah, D. Yang, R. Piner, A. Velamakanni, I. Jung, E. Tutuc, S.K. Banerjee, L. Colombo, R.S. Ruoff, Science 324 (2009) 1312–1314.
[10] K.S. Kim, Y. Zhao, H. Jang, S. Lee, J.M. Kim, K.S. Kim, mJ.-H. Ahn, P. Kim, J.-Y. Choi, B.H. Hong, Nature 457 (2009) 706–710.
[11] A. Reina, X. Jia, J. Ho, D. Nezich, H. Son, V. Bulovic, M.S. Dresselhaus, J. Kong, Nano Lett. 9 (2009) 3087.
[12] A.H.C. Neto, F. Guinea, N.M.R. Peres, K.S. Novoselov, A.K. Geim, Rev. Mod. Phys. 81 (2009) 109.
[13] L. Gao, W. Ren, H. Xu, L. Jin, Z. Wang, T. Ma, L.-P. Ma, Z. Zhang, Q. Fu, L.-M. Peng, X. Bao, H.-M. Cheng, Nat. Commun. 3-699 (2012) 1.
[14] J. Coraux, A.T.N. Diaye, M. Engler, C. Busse, D. Wall, N. Buckanie, F.-J.M. zu Heringdorf, R. van Gastel, B. Poelsema, T. Michely, N. J. Phys. 11 (2009) 023006.
[15] E. Loginova, N.C. Bartelt, P.J. Feibelman, K.F. McCarty, N. J. Phys. 10 (2008) 093026.
[16] T. Oznuluer, E. Pince, E.O. Polat, O. Balci, O. Salihoglu, C. Kocabas, Appl. Phys. Lett. 98 (2011) 183101.
[17] D. Prasai, J.C. Tuberquia, R.R. Harl, G.K. Jennings, K.I. Bolotin, ACS Nano 6 (2012) 1102–1108.
[18] Z. Yan, Y. Liu, L. Ju, Z. Peng, J. Lin, G. Wang, H. Zhou, C. Xiang, E.L. G. Samuel, C. Kittrell, V.I. Artyukhov, F. Wang, B.I. Yakobson, J.M. Tour, Angew. Chem. 53 (2014) 1565–1569.
[19] Y. Zhang, T.-T. Tang, C. Girit, Z. Hao, M.C. Martin, A. Zettle, M.F. Crommie, Y.R. Shen, F. Wang, Nature 459 (2009) 820–823.
[20] J.B. Oostinga, H.B. Heersche, X. Liu, A.F. Morpurgo, L.M. K. Vandersypen, Nat. Mater. 7 (2008) 151–157.
[21] T. Ohta, A. Bostwick, T. Seyller, K. Horn, E. Rotenberg, Science 313 (2006) 951–954.
[22] K.F. Mak, C.H. Lui, J. Shan, T.F. Heinz, Phys. Rev. Lett. 102 (2009) 256405.
[23] A. Luican, G. Li, A. Reina, J. Kong, R.R. Nair, K.S. Novoselov, A.K. Geim, E.Y. Andrei, Phys. Rev. Lett. 106 (2011) 126802.
[24] J.W. Suk, A. Kitt, C.W. Magnuson, Y. Hao, S. Ahmed, J. An, A.K. Swan, B.B. Goldberg, R.S. Ruoff, ACS Nano 5 (9) (2011) 6916–6924.
[25] X. Li, Y. Zhu, W. Cai, M. Borysiak, B. Han, D. Chen, R.D. Piner, L. Colombo, R.S. Ruoff, Nano Lett. 9 (2009) 4359–4363.
[26] Y. Wang, S.W. Tong, X.F. Xu, B. Özyilmaz, K.P. Loh, Adv. Mater. 23 (13) (2011) 1514–1518.
[27] Z. Yan, J. Lin, Z. Peng, Z. Sun, Y. Zhu, L. Li, C. Xiang, E.L. Samuel, C. Kittrell, J.M. Tour, ACS Nano 6 (10) (2012) 9110.
[28] ⟨http://www.nanomagnetics-inst.com/en/products/ambient-microscopes/high-performance-afmmfm-hpafm⟩.
[29] A.W. Robertson, J.H. Warner, Nano Lett. 11 (2011) 1182.
[30] V.I. Artyukhov, Y. Liu, B.I. Yakobson, Proc. Natl. Acad. Sci. USA 109 (2012) 15136–15140.
[31] A. Charles, Bishop, Vacuum Deposition onto Webs, Films, and Foils, William Andrew Publishing, Norwich NY, USA, 2006.
[32] Y. Hao, M.S. Bharathi, L. Wang, Y. Liu, H. Chen, S. Nie, X. Wang, H. Chou, C. Tan, B. Fallahazad, H. Ramanarayan, C.W. Magnuson, E. Tutuc, B.I. Yakobson, K.F. McCarty, Y.W. Zhang, P. Kim, J. Hone, L. Colombo, R.S. Ruoff, Science 342 (2013) 720.
[33] X. Li, C.W. Magnuson, A. Venugopal, J. An, J.W. Suk, B. Han, M. Borysiak, W. Cai, A. Velamakanni, Y. Zhu, L. Fu, E.M. Vogel, E. Voelkl, L. Colombo, R.S. Ruoff, Nano Lett. 10 (2010) 4328.
[34] Z. Yan, Z. Peng, J.M. Tour, Acc. Chem. Res. 47 (2014) 1327.
[35] H. Zhou, W.J. Yu, L. Liu, R. Cheng, Y. Chen, X. Huang, Y. Liu, Y. Wang, Y. Huang, X. Duan, Nat. Commun. 4 (2013) 2096.
[36] X. Li, W. Cai, L. Colombo, R.S. Ruoff, Nano Lett. 9 (2009) 4268–4272.
[37] S. Nie, W. Wu, S. Xing, Q. Yu, J. Bao, S-s Pei, K.F. McCarty, N. J. Phys. 14 (2012) 093028.

[38] A. Pimpinelli, J. Villain, Physics of Crystal Growth, Cambridge University Press, Cambridge, 1998.
[39] A.Y. Tontegode, Prog. Surf. Sci. 38 (1991) 201–429.
[40] S. Nie, A.L. Walter, N.C. Bartelt, E. Starodub, A. Bostwick, E. Rotenberg, K.F. McCarty, ACS Nano 5 (2011) 2298–2306.
[41] Y. Cui, Q. Fu, X. Bao, Phys. Chem. Chem. Phys. 12 (2010) 5053–5057.
[42] W. Fang, A.L. Hsu, R. Caudillo, Y. Song, A.G. Birdwell, E. Zakar, M. Kalbac, M. Dubey, T. Palacios, M.S. Dresselhaus, P.T. Araujo, J. Kong, Nano Lett. 13 (2013) 1541–1548.
[43] S. Gayathri, P. Jayabal, M. Kottaisamy, V. Ramakrishnan, AIP Adv. 4 (2014) 027116.
[44] E.A. Obraztsova, A.V. Osadchy, E.D. Obraztsova, S. Lefrant, I.V. Yaminsky, Phys. Stat. Sol. (b) 245 (2008) 2055–2059.
[45] A.C. Ferrari, Solid Stat. Commun. 143 (2007) 47–57.
[46] Y. Hao, Y. Wang, L. Wang, Z. Ni, Z. Wang, R. Wang, C.K. Koo, Z. Shen, J.T.L. Thong, Small 6 (2010) 195–200.
[47] L.M. Malard, J. Nilsson, D.C. Elias, J.C. Brant, F. Plentz, E.S. Alves, A.H. Castro Neto, M.A. Pimenta, Phys. Rev. B 76 (2007) 201401 R.
[48] L. Liu, H. Zhou, R. Cheng, W.J. Yu, Y. Liu, Y. Chen, J. Shaw, X. Zhong, Y. Huang, X. Duan, ACS Nano 6 (9) (2012) 8241–8249.
[49] T.E. Beechem, T. Ohta, B. Diaconescu, J.T. Robinson, ACS Nano 8 (2) (2014) 1655–1663.
[50] K. Kim, S. Coh, L.Z. Tan, W. Regan, J.M. Yuk, E. Chatterjee, M.F. Crommie, M.L. Cohen, S.G. Louie, A. Zettl, Phys. Rev. Lett. 108 (2012) 246103.
[51] J. Zhang, J. Zhao, J. Appl. Phys. 113 (2013) 043514–043514-5.
[52] J.-K. Lee, S.-C. Lee, J.-P. Ahn, S.-C. Kim, J.I.B. Wilson, P. John, J. Chem. Phys. 129 (2008) 234709.